Mapping excitons in semiconducting carbon nanotubes with plasmonic nanoparticles

Jürgen Waxenegger, Andreas Trügler, and Ulrich Hohenester*
Institut für Physik, Karl-Franzens-Universität Graz, Universitätsplatz 5, A-8010 Graz, Austria
(Received 9 July 2010; revised manuscript received 16 May 2011; published 28 June 2011)

We develop a consistent theoretical framework suited for the description of confined-exciton mapping in semiconducting carbon nanotubes, using apertureless scanning near-field optical microscopy. In the proposed experimental setup, a plasmonic nanoparticle, such as a nanosphere, is scanned over the nanotube, and the scattered light is recorded. The presence of the plasmonic nanoparticle modifies the excitation channel as well as the dielectric environment, which can be exploited to extract information about the confined excitons. From our simulations, we identify characteristic features observable in experiment.

DOI: 10.1103/PhysRevB.83.245446 PACS number(s): 73.20.Mf, 71.35.−y, 68.37.Uv, 78.67.Ch

I. INTRODUCTION

Optical microscopy provides a unique means for remote measurements but generally lacks spatial resolution on the nanometer scale. A noticeable exception is scanning near-field optical microscopy (SNOM).[1] In aperture SNOM, the uncoated apex of a sharply pointed optical fiber represents an aperture through which the sample is excited by light (illumination mode) or light emitted by the sample is detected (collection mode). Alternatively, in apertureless SNOM, optical antenna structures, usually based on plasmonic nanostructures, convert electromagnetic near fields to far-field radiation or vice versa. Both approaches operate in the near-field regime and thus allow us to overcome the diffraction limit of light, thereby achieving spatial resolutions of the order of tens of nanometers.

Near-field microscopy has been used successfully for the measurement of semiconductor quantum dots,[2–4] molecules,[5,6] and carbon nanotubes.[7–11] While all these studies have used SNOM only to locate the nanostructures and to extract spectroscopic information on the isolated nano objects, Matsuda and co-workers[12] proceeded one step further by mapping out the *wave function* of an exciton in a semiconductor quantum dot. The confinement was induced by the local monolayer fluctuations in the thickness of a semiconductor quantum well, leading to wave-function extensions of about 100 nm, which is significantly larger than the spatial resolution of aperture SNOM. Under these conditions, it becomes indeed possible to "look" into the confined wave functions.[12–17]

The situation is more adverse for other nano structures, such as carbon nanotubes (CNT's), which have recently received enormous interest, since typical extensions of exciton wave functions confined by nanotube bending or DNA wrapping[10] are expected to be of the order of or below the spatial resolution of aperture SNOM. Apertureless SNOM appears to be more promising for exciton mapping in nanotubes, as plasmonic nanoparticles allow to focus electromagnetic fields down to spots with sizes of a few nanometers.[18] On the other hand, the plasmonic particle also leads to a modification of the photonic local density of states (LDOS), which, in principle, makes it difficult to disentangle the effects of excitation, radiative decay, and the change of the exciton confinement potential. Although SNOM has been used for detection of excitons in CNT's,[7–11] to the best of our knowledge thus far no mapping of the underlying wave functions has been achieved.

In this paper, we develop a theoretical framework suited for the description of apertureless exciton mapping in semiconducting CNT's, and we predict characteristic features observable in experiment. We find that the presence of a plasmonic nanoparticle distorts the CNT exciton wave function through the modification of the dielectric environment, and that quantum interference leads to an enhancement or suppression of the scattered light intensity, which depends strongly on the light polarization. These features provide clear fingerprints of confined excitons in CNT's. On the other hand, because of the strong coupling between the nanotube excitons and the plasmonic nanoparticle, in apertureless SNOM one is probing the properties of the coupled system rather than those of the isolated excitons, which hinders a clear-cut and unambiguous wave-function mapping.

We have organized our paper as follows. In Sec. II, we introduce our theoretical framework based on the semiconductor Bloch equations and the rigid exciton approximation. Our approach naturally includes the modification of the excitation channel and the change of the dielectric environment induced by the plasmonic nanoparticle. Simulation results for a spherical gold nanoparticle are presented in Sec. III. Finally, in Sec. IV we summarize and draw some conclusions.

II. THEORY

A. Semiconductor Bloch equations

In our theoretical approach, we start from the semiconductor Bloch equations,[19] which describe the dynamics of an electron-hole pair in the presence of a confinement potential and laser excitation in terms of the *interband polarization*,

$$p(\boldsymbol{r}_e,\boldsymbol{r}_h) = \langle \hat{\Psi}_h(\boldsymbol{r}_h)\hat{\Psi}_e(\boldsymbol{r}_e)\rangle\,. \tag{1}$$

Here $\hat{\Psi}^\dagger_{e,h}(\boldsymbol{r})$ is the field operator that excites an electron or hole at position $\boldsymbol{r}$. At sufficiently low excitation powers, the expression given in Eq. (1) is the leading term, and higher-order contributions such as the electron and hole densities can be neglected.[20] In our approach, we use envelope functions[19] and assume effective masses $m_{e,h}$ for the electron and hole. The equation of motion for the interband polarization then follows

from the Heisenberg equations of motion, and one obtains (we set $\hbar = 1$)

$$i\,\dot{p}(\boldsymbol{r}_e,\boldsymbol{r}_h) = -\delta(\boldsymbol{r}_e-\boldsymbol{r}_h)\,\Omega(\boldsymbol{r}_e,t) + \left(\sum_{i=e,h}\left[-\frac{\nabla_i^2}{2m_i}+U_i(\boldsymbol{r}_i)\right]+V_{eh}(\boldsymbol{r}_e-\boldsymbol{r}_h)\right)p(\boldsymbol{r}_e,\boldsymbol{r}_h). \quad (2)$$

The first term on the right-hand side describes the creation of electron-hole pairs through coupling to the external laser. We have used the rotating-wave approximation, and we describe the light-matter coupling within the dipole approximation in terms of the Rabi energy[21] $\Omega(\boldsymbol{r},t)$. As will be discussed below, Ω includes both the direct coupling through an external light field and modifications of the photonic LDOS through a plasmonic nanoparticle. The second term on the right-hand side accounts for the kinetic energies of the electron and hole, their confinement potentials $U_{e,h}$, which are assumed to be induced by nanotube bending or modifications of the dielectric environment, e.g., through DNA wrapping, and V_{eh} accounts for the attractive electron-hole Coulomb interaction.

In what follows, we employ the rigid-exciton approximation,[14,22] which assumes that the electron-hole wave function can be separated into two parts, depending on the relative and center-of-mass coordinates, respectively. This approximation is valid when the exciton Bohr radius is significantly smaller than the spatial variations of the confinement potential. In more detail, let

$$\left(-\frac{\nabla_\rho^2}{2\mu}+V_{eh}(\boldsymbol{\rho})\right)\phi_0(\boldsymbol{\rho}) = \epsilon_0\phi_0(\boldsymbol{\rho}) \quad (3)$$

be the solution of the exciton Schrödinger equation in the absence of a confinement potential (μ is the reduced electron-hole mass). Here and in the following, we assume that for sufficiently low photon energies, only the ground state of Eq. (3) has to be considered. When $U_i(\boldsymbol{r}_i)$ varies smoothly on the length scale of the excitonic Bohr radius,[19,23,24] which is governed by the spatial variations of $\phi_0(\boldsymbol{\rho})$, the interband polarization in Eq. (2) can be approximated as

$$p(\boldsymbol{r}_e,\boldsymbol{r}_h) \cong \mathcal{P}(\boldsymbol{R})\,\phi_0(\boldsymbol{\rho}), \quad (4)$$

with $\mathcal{P}(\boldsymbol{R})$ being the exciton envelope function that only depends on the center-of-mass coordinate $\boldsymbol{R}$. Throughout, we shall refer to $\mathcal{P}(\boldsymbol{R})$ as the *exciton wave function*. Equation (4) describes an electron-hole pair that is tightly bound by the attractive Coulomb interaction, and the confinement potential only affects the center-of-mass motion but has otherwise no impact on the internal structure of the exciton.

Upon insertion of the product ansatz of Eq. (4) into the equation of motion for the interband polarization, Eq. (2), we obtain after some simple modifications

$$i\dot{\mathcal{P}}(\boldsymbol{R}) = -\phi_0(0)\,\Omega(\boldsymbol{R},t)+\left(-\frac{\nabla_R^2}{2M}+V(\boldsymbol{R})\right)\mathcal{P}(\boldsymbol{R}). \quad (5)$$

Here $M = m_e + m_h$ is the exciton mass, and the effective confinement potential reads

$$V(\boldsymbol{R}) = \int\left[V_e\left(\boldsymbol{R}+\frac{\boldsymbol{\rho}}{2}\right)+V_h\left(\boldsymbol{R}-\frac{\boldsymbol{\rho}}{2}\right)+\epsilon_0\right]\phi_0^2(\boldsymbol{\rho})\,d\boldsymbol{\rho}\,. \quad (6)$$

B. CNT excitons

We next introduce a few modifications suited for the description of excitons in carbon nanotubes. First, we assume that the center-of-mass motion only depends on the longitudinal z direction along the nanotube. The transversal degrees of freedom have been integrated out in our approach, and enter only indirectly through ϵ_0 and $\phi_0(\boldsymbol{\rho})$. Second, we assume that there exist three types of excitons with dipole moments $\boldsymbol{d}_\lambda$ oriented along the longitudinal and transversal directions, respectively.[25,26] For simplicity, we assume that all excitons have the same wave function $\phi_0(\boldsymbol{\rho})$. Then, the equations of motion for the envelope functions become

$$i\dot{\mathcal{P}}_\lambda(z) = -\boldsymbol{d}_\lambda\cdot\boldsymbol{E}(z,t)+\left(-\frac{\partial_z^2}{2M}+V(z)\right)\mathcal{P}_\lambda(z). \quad (7)$$

The total polarization of the CNT excitons is obtained by summing over all interband polarizations viz.

$$\boldsymbol{P}(z,t) = \sum_\lambda \boldsymbol{d}_\lambda\,\mathcal{P}_\lambda(z,t). \quad (8)$$

While for the isolated nanotube these three fundamental modes are decoupled, in the case of a modified photonic environment they become mixed, as will be discussed in the following.

C. Modification of photonic LDOS

We next ponder the interaction of the CNT excitons with a nearby plasmonic nanoparticle. The situation we have in mind is schematically depicted in Fig. 1. A plasmonic nanoparticle, such as a metallic nanosphere, is brought into the vicinity

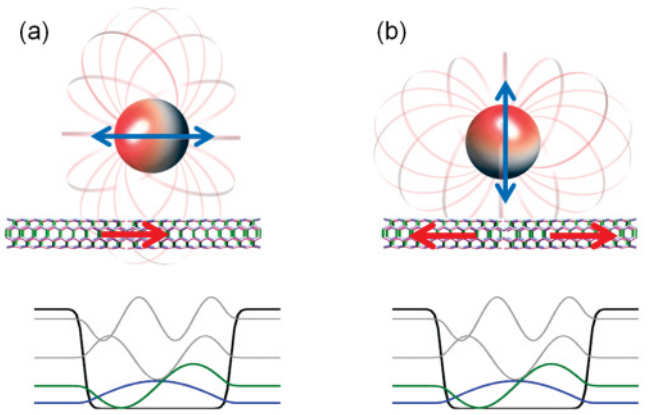

FIG. 1. (Color online) Schematics of the mapping of CNT excitons with a plasmonic nanoparticle. In the lower part of the panels, we depict our generic boxlike confinement potential and the confined exciton states. In the upper part, we sketch the electric-field distribution produced by the surface plasmons of the metallic nanoparticle. (a) For light polarization *parallel* to the nanotube symmetry axis, the CNT exciton can be directly excited or via the nanoparticle. The arrows indicate the dipole moments of the nanoparticle and the exciton. (b) For *perpendicular* light polarization, the exciton can only be excited via the plasmonic nanoparticle. The near fields of the nanoparticle, schematically shown in the figure, are such that the induced exciton dipole moments on the left- and right-hand side of the nanoparticle point into opposite directions.

of a carbon nanotube. For sufficiently small distances, say below 10 nm, the presence of the plasmonic nanoparticle has two important effects. First, when the system is excited by far-field radiation, the metallic nanoparticle focuses light down to a nanometer spot, and thus noticeably alters the optical excitation and decay channels. In addition, it modifies the dielectric environment for the CNT excitons.

To account for these modifications, we introduce a theoretical approach similar to that of Ref. 27, where the authors investigated hybrid modes of plasmonic nanoparticles and quantum emitters, described in terms of localized dipoles. In our situation, things are slightly more complicated since the CNT excitons are delocalized, which leads to additional quantum coherence effects. More specifically, the electric field $\boldsymbol{E}(z,t)$ impinging on the nanotube consists of one part $\boldsymbol{E}_{\rm inc}$ associated with the external laser (including the excitation modification by the plasmonic nanoparticle) and another part associated with the modification of the dielectric environment. For the latter part, we assume a self-interaction where the electric field, created by the polarization, acts back on the exciton viz.

$$\boldsymbol{E}_{\rm ind}(z,\omega) = k^2 \int \boldsymbol{G}_{\rm refl}(z,z',\omega)\cdot\boldsymbol{P}(z',\omega)\,dz' . \qquad (9)$$

Here $k=\omega/c$ is the wave number of light and $\boldsymbol{G}_{\rm refl}(z,z',\omega)$ is the dyadic Green function,[1] which gives the electric field at position z for a dipole source located at position z'. The reflected part $\boldsymbol{G}_{\rm refl}$ differs from the total Green function in that the free-space contribution has been subtracted. In Eq. (9), we have performed a Fourier transformation in time. Introducing this expression into Eq. (7), we arrive at our final expression,

$$\omega\mathcal{P}_\lambda(z) = -\boldsymbol{d}_\lambda\cdot\boldsymbol{E}_{\rm inc}(z,t) + \left(-\frac{\partial_z^2}{2M}+V(z)\right)\mathcal{P}_\lambda(z) - k^2\sum_{\lambda'}\int \boldsymbol{d}_\lambda\cdot\boldsymbol{G}_{\rm refl}(z,z',\omega)\cdot\boldsymbol{d}_{\lambda'}\,\mathcal{P}_{\lambda'}(z')\,dz' . \qquad (10)$$

It describes the excitation and propagation of excitons in carbon nanotubes in the presence of an exciting laser and of a plasmonic nanoparticle. The first term on the right-hand side is a source term accounting for the exciton creation through the external laser. The second term describes the exciton propagation in the presence of a confinement potential, and the last term describes the modification of the dielectric confinement through the plasmonic nanoparticle. Here the exciton polarizes the plasmonic nanoparticle, and the polarization acts back on the exciton.

D. Plasmonic nanoparticle

Thus far we have derived an equation of motion for the exciton polarization. All effects of the plasmonic nanoparticle are embodied in the modified exciting field $\boldsymbol{E}_{\rm inc}$ and the reflected part $\boldsymbol{G}_{\rm refl}$ of the dyadic Green function. The calculation of $\boldsymbol{G}_{\rm refl}$ can be simplified considerably if we perform the *quasistatic approximation*,[1,28,29] which assumes that the size L of the metallic nanoparticle is much smaller than the light wavelength λ, i.e., $L \ll \lambda$. For spherical nanoparticles, we can then compute the nanoparticle response analytically.[27,30] In our computational approach, we rather use an eigenmode expansion within a boundary element method approach,[28,29,31,32] which, in principle, can be used for plasmonic nanoparticles of arbitrary shape. However, as we will only be concerned here with spherical nanoparticles, we will not enter into the details of this approach.

III. RESULTS

A. Model system and simulation

In our simulations, we consider a gold nanosphere with a diameter of 10 nm.[33] Smaller sphere diameters might be beneficial for achieving more localized electromagnetic fields, and correspondingly a higher spatial resolution in apertureless SNOM experiments, but they would render the experiment prohibitively difficult. The dielectric function of the metal is taken from experiment,[34] and we assume a background with a refractive index of $n_b = 1.5$.

For the exciton, we take parameters representative of (8,0) semiconducting CNT's,[26] with an energy gap of 1.55 eV and a dipole moment of four atomic units along the nanotube direction. The latter is estimated from *ab initio* calculations for the dipole matrix element[26] and for an exciton wave function with[23,24] $\phi(0)=\sqrt{8/\pi}$. The dipole moments along the perpendicular directions are set to zero. We checked that finite but small values, say 10% of the parallel component, did not change our results.

We consider a generic boxlike potential for the exciton confinement, shown in the inset of Fig. 1, with a confinement length of $L_0 = 40$ nm and a depth of $V_0 = 20$ meV. This results in a number of confined exciton states whose shapes are reminiscent of a particle in a box. Such confinement could be achieved through nanotube bending or DNA wrapping.[10] Alternatively, in a slightly different setup, one could also use electrical gates for confining charged excitons.[35] We have chosen L_0 of the order of the plasmonic nanoparticle, and correspondingly of the plasmonic near fields, to be able to detect spatial variations of the exciton states. As for V_0, we checked that larger or somewhat smaller values, say around $V_0 = 10$ meV, would not significantly alter our results. Thus, our approach is expected to mimic the effect of a generic exciton confinement.

In our simulations, we solve Eq. (10) by discretizing $\mathcal{P}_\lambda(z)$, $V(z)$, and $\boldsymbol{G}_{\rm refl}(z,z',\omega)$ in space (with a typical number of 100 z values) and solving the resulting matrix equation through inversion for each photon energy ω and for each position of the metallic nanoparticle. From the solutions $\mathcal{P}_\lambda(z)$, we finally compute the scattered light intensity using the sum of the exciton and plasmonic nanoparticle dipole moments.[29,32]

B. Mapping with the plasmonic nanoparticle

Figure 2 shows our computed scattering spectra for a distance between the CNT and the plasmonic nanoparticle of (a,b) 5 and (c,d) 10 nm. The left column [panels (a,c)] reports results where the incoming laser light is polarized along the CNT direction, and the right column [panels (b,d)] for a light polarization perpendicular to the nanotube. Let us first concentrate on the results of parallel polarization.

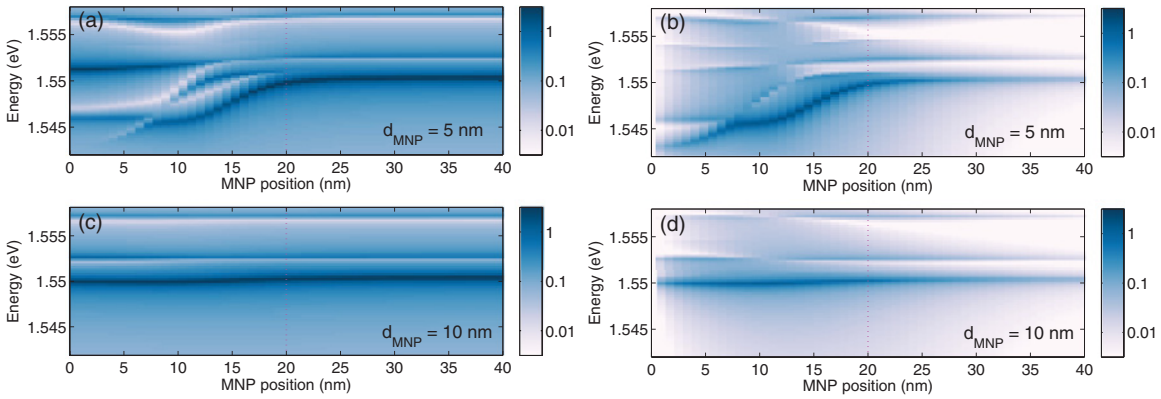

FIG. 2. (Color online) Simulated light-scattering spectra for the setup depicted in Fig. 1 and for light polarization (a,c) parallel and (b,d) perpendicular to the CNT symmetry axis, and for a nanoparticle-CNT distance of (a,b) 5 nm and (c,d) 10 nm. We plot the normalized spectra and use a logarithmic color scale. For the smaller distance, panels (a,b), we observe a pronounced redshift of the scattering peaks when the plasmonic nanoparticle comes close to the confined exciton.

1. Parallel polarization

For all nanoparticle positions, we observe at least two spectral positions where the scattered light intensity is strong. These spectral positions are associated with the ground and excited states of the confined exciton. It is important to realize that for the small nanosphere under investigation and the large detuning with respect to the plasmon energy (the plasmonic dipole modes of the sphere are around 2.4 eV), the direct light absorption and emission by the CNT exciton is significantly larger than the indirect processes, where the excited laser light is focused by the nanoparticle and the CNT exciton uses the metallic nanoparticle as a nano antenna in order to emit more efficiently. As direct absorption and emission dominate over the indirect processes, the intensity of the scattered light does not depend noticeably on the nanoparticle position.

We observe a redshift of the peak positions when the nanoparticle is located in the region of the confinement potential. This shift is more pronounced for the smaller nanoparticle-CNT distance; see panel (a) of the figure. To understand more closely its origin, in Fig. 3(a) we plot the polarization $\mathcal{P}_z(z)$, extracted from our simulations at the frequency corresponding to the peak at the lowest energy in the trap center. One observes that the maximum of $\mathcal{P}_z(z)$ closely follows the metallic nanoparticle. This is because of the self-interaction induced by $\boldsymbol{G}_{\rm refl}(z,z',\omega)$, which can be interpreted in terms of a simple image-charge model:[30] the CNT dipole distribution $\boldsymbol{d}_z\,\mathcal{P}_z(z)$ below the nanosphere induces a mirror dipole within the metallic nanosphere, which acts as an attractive potential for the exciton. Thus, the confined exciton is energetically shifted and becomes slightly deformed in the presence of the plasmonic probe. The energy renormalization is strongly diminished when the nanoparticle-CNT distance is increased; see Fig. 2(c).

2. Perpendicular polarization

Things change considerably when the polarization of the incoming light is perpendicular to the CNT axis. In this case, direct light excitation is not possible (or at least strongly suppressed, because of the much weaker perpendicular dipole moments). Excitation is now an indirect process, where the laser excites the CNT exciton via the near fields of the plasmonic nanoparticle. Indeed, in Figs. 2(b) and 2(d) we observe that light scattering only occurs when the nanosphere is located close to the confined exciton. Again, we observe a redshift attributed to the image-charge attraction.

In Fig. 3(b), we show the corresponding polarization distribution $\mathcal{P}_z(z)$. We find that the distribution has a node underneath the nanosphere, whose origin is due to interference. Suppose that the nanoparticle is located at $z = 0$ and becomes excited by light with polarization along x. The induced near field along z then points to opposite directions for positive and negative z values, respectively, as schematically shown in Fig. 1(b). Below the nanosphere, the near field has no component along the nanotube axis, and the polarization becomes zero; see Fig. 3(b). An electric field of such shape cannot excite the exciton ground-state potential because of symmetry reasons, as evidenced by the vanishing light-scattering intensity depicted in Fig. 2(b). When moving away from the center of the confinement potential, symmetry becomes broken, which leads to a noticeable scattering from all CNT excitons. Although there is a rich structure in the spectral maps, we were not able to unambiguously relate the different features to specific properties of the underlying exciton states. For instance, the crossing of the lowest and first excited polariton states around $z \approx 7$ nm is related to the mixing of the ground and excited exciton states with even and odd parity, respectively. Close to the center of the confinement potential, i.e., around $z \approx 0$, the character of the polariton is governed by the first excited exciton state with odd parity.

IV. CONCLUSIONS

In the previous section, we showed that the mapping of CNT excitons with plasmonic nanoparticles is feasible and can provide detailed information about the exciton states. A pronounced polarization dependence and an energy shift of the scattering peaks, induced by the modification of the dielectric environment through the plasmonic probe, are the most striking features predicted from our simulations.

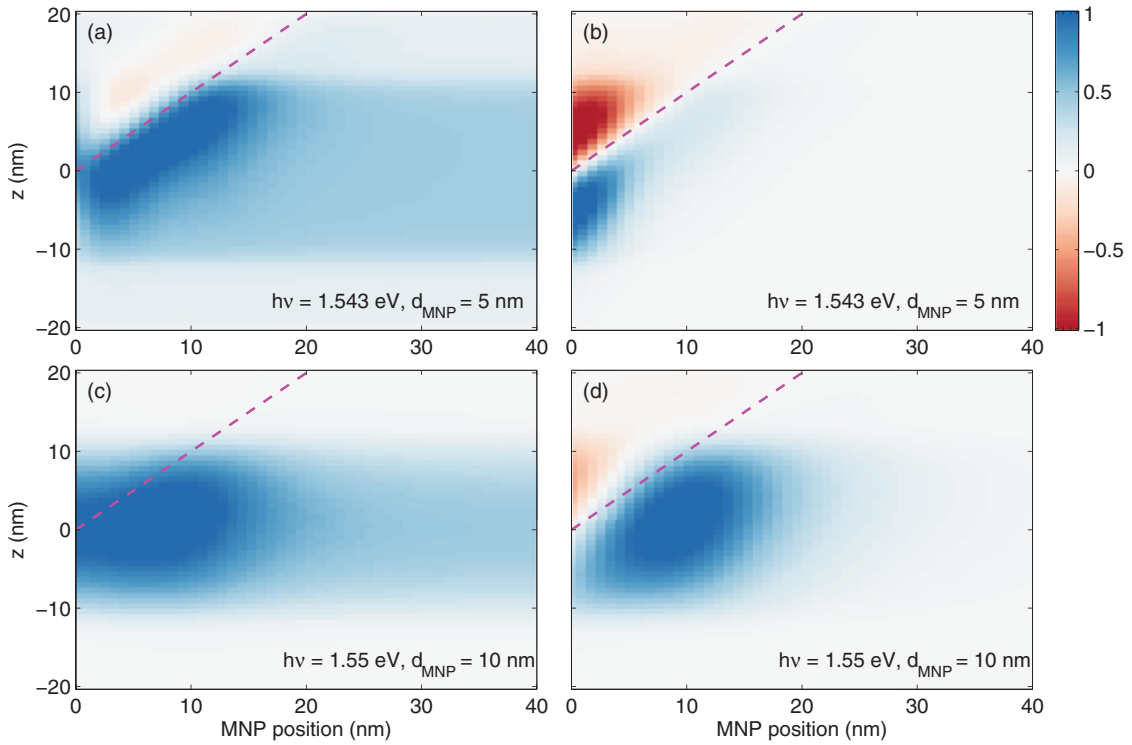

FIG. 3. (Color online) Real part of polarization $\mathcal{P}_z(z)$ (i.e., "exciton wave function") in arbitrary units, as obtained from our simulations, at the scattering maxima of lowest energy in the trap center (photon energies are given in the panels) and for different nanoparticle positions. The setups for the different panels correspond to those of Fig. 2, and the dashed lines indicate the positions of the metallic nanoparticle. For parallel light polarization and a small MNP-CNT distance, panel (a), we observe an attractive interaction (due to the induced image dipole), and the maximum of $\mathcal{P}_z(z)$ follows the plasmonic nanoparticle. (b) For perpendicular polarization, the wave function has a node below the plasmonic nanoparticle, as a result of the excitation via the surface-plasmon fields depicted in Fig. 1(b).

On the other hand, from our simulations we were not able to extract clear-cut information about the underlying exciton *wave functions*, as would have been evidenced, e.g., by observing the nodes of the excited exciton states. The perturbation of the photonic LDOS by the plasmonic nanoparticle appears to be so strong that the excitons behave more like a polarizable medium than a genuine quantum-mechanical object. The situation would be even more adverse for larger confinement lengths L_0, whereas for smaller L_0 the spatial resolution of the plasmonic probe would not suffice to detect spatial details of the exciton wave functions.

In this work, we have focused on small nanoparticles and strongly off-resonant plasmon modes, which makes the interpretation of our results more simple. Preliminary calculations for resonant structures, e.g., ellipsoids reminiscent of sharp metallic tips, revealed a rich variety of effects in the optical spectra, which can be partially attributed to strong modifications in the excitation and emission channels. On the other hand, we expect that the setup described in this work is conceptually more simple but still capable of retrieving the relevant information about confined excitons in carbon nanotubes.

In most experiments with CNT's, dark excitons originating from the singlet-triplet splitting strongly quench the exciton luminescence.[26,36] Such quenching is not crucial in our situation since we have investigated coherent light scattering. Nevertheless, it could be interesting to investigate whether the nanoparticle-induced modification of the dielectric environment could modify the emission channel for the dark triplet excitons, although such analysis is beyond the scope of our present work. Our theoretical approach, in principle, includes nonradiative losses, due to Ohmic dissipation in the metallic nanoparticle, as well as excitation of dark states, whose excitation becomes possible due to the breaking of the usual optical selection rules through near-field excitation, but we have refrained from an explicit discussion of these issues.

In conclusion, we have introduced a consistent theoretical framework suited for the description of apertureless SNOM measurements of confined excitons in carbon nanotubes. Our approach is based on the optical Bloch equations and the rigid exciton approximation, and includes the modification of the excitation channel as well as the dielectric environment induced by the plasmonic nanoparticle. We have performed simulations for a spherical gold nanoparticle and a generic boxlike confinement potential, and we have demonstrated that mapping of confined CNT excitons is indeed possible with apertureless SNOM. We hope that our results will stimulate further experiments in this direction.

*ulrich.hohenester@uni-graz.at

[1] L. Novotny and B. Hecht, *Principles of Nano-Optics* (Cambridge University Press, Cambridge, 2006).

[2] E. Betzig, J. K. Trautman, T. D. Harris, J. S. Weiner, and R. L. Kostelak, Science **251**, 1468 (1991).

[3] H. F. Hess, E. Betzig, T. D. Harris, L. N. Pfeiffer, and K. W. West, Science **264**, 1740 (1994).

[4] J. R. Guest, T. H. Stievater, G. Chen, E. A. Tabak, B. G. Orr, D. G. Steel, D. Gammon, and D. S. Katzer, Science **293**, 2224 (2001).

[5] W. E. Moerner, T. Plakhotnik, T. Irngartinger, U. P. Wild, D. W. Pohl, and B. Hecht, Phys. Rev. Lett. **73**, 2764 (1994).

[6] C. Hettich, C. Schmitt, J. Zitzmann, S. Kühn, I. Gerhardt, and V. Sandoghdar, Science **298**, 385 (2002).

[7] A. Hartschuh, E. J. Sánchez, X. S. Xie, and L. Novotny, Phys. Rev. Lett. **90**, 095503 (2003).

[8] A. Hartschuh, H. Qian, A. J. Meixner, N. Anderson, and L. Novotny, Nano. Lett. **5**, 2310 (2005).

[9] A. Hartschuh, H. Qian, A. J. Meixner, N. Anderson, and L. Novotny, J. Lumin. **119-120**, 204 (2006).

[10] H. Qian, P. T. Araujo, C. Georgi, T. Gorkus, N. Hartmann, A. A. Green, A. Jorio, M. C. Hersam, L. Novotny, and A. Hartschuh, Nano Lett. **8**, 2706 (2008).

[11] T. Ichimura, S. Fujii, P. Verma, T. Yano, Y. Inouye, and S. Kawata, Phys. Rev. Lett. **102**, 186101 (2009).

[12] K. Matsuda, T. Saiki, S. Nomura, M. Mihara, Y. Aoyagi, S. Nair, and T. Takagahara, Phys. Rev. Lett. **91**, 177401 (2003).

[13] C. D. Simserides, U. Hohenester, G. Goldoni, and E. Molinari, Phys. Rev. B **62**, 13657 (2000).

[14] U. Hohenester, G. Goldoni, and E. Molinari, Appl. Phys. Lett. **84**, 3963 (2004).

[15] U. Hohenester, G. Goldoni, and E. Molinari, Phys. Rev. Lett. **95**, 216802 (2005).

[16] E. Runge and C. Lienau, Phys. Rev. B **71**, 035347 (2005).

[17] L. He, G. Bester, Z. Su, and A. Zunger, Phys. Rev. B **76**, 035313 (2007).

[18] S. A. Maier, *Plasmonics: Fundamentals and Applications* (Springer, Berlin, 2007).

[19] H. Haug and S. W. Koch, *Quantum Theory of the Optical and Electronic Properties of Semiconductors* (World Scientific, Singapore, 1993).

[20] V. M. Axt and S. Mukamel, Rev. Mod. Phys. **70**, 145 (1998).

[21] M. O. Scully and M. S. Zubairy, *Quantum Optics* (Cambridge University Press, Cambridge, UK, 1997).

[22] R. Zimmermann, F. Große, and E. Runge, Pure Appl. Chem. **69**, 1179 (1997).

[23] T. G. Pedersen, Phys. Rev. B **67**, 073401 (2003).

[24] D. Kammerlander, D. Prezzi, G. Goldoni, E. Molinari, and U. Hohenester, Phys. Rev. Lett. **99**, 126806 (2007).

[25] E. Chang, G. Bussi, A. Ruini, and E. Molinari, Phys. Rev. Lett. **92**, 196401 (2004).

[26] C. D. Spataru, S. Ismail-Beigi, R. B. Capaz, and S. G. Louie, Phys. Rev. Lett. **95**, 247402 (2005).

[27] W. Zhang, A. O. Govorov, and G. W. Bryant, Phys. Rev. Lett. **97**, 146804 (2006).

[28] F. J. Garcia de Abajo and A. Howie, Phys. Rev. B **65**, 115418 (2002).

[29] U. Hohenester and A. Trügler, IEEE J. Sel. Top. Quantum Electron. **14**, 1430 (2008).

[30] J. D. Jackson, *Classical Electrodynamics* (Wiley, New York, 1999).

[31] U. Hohenester and J. R. Krenn, Phys. Rev. B **72**, 195429 (2005).

[32] A. Trügler and U. Hohenester, Phys. Rev. B **77**, 115403 (2008).

[33] P. Anger, P. Bharadwaj, and L. Novotny, Phys. Rev. Lett. **96**, 113002 (2006).

[34] P. B. Johnson and R. W. Christy, Phys. Rev. B **6**, 4370 (1972).

[35] R. Matsunaga, K. Matsuda, and Y. Kanemitsu, Phys. Rev. Lett. **106**, 037404 (2011).

[36] F. Wang, G. Dukovic, L. E. Brus, and T. F. Heinz, Phys. Rev. Lett. **92**, 177401 (2004).